Chem Soc Rev

The Dynamic, Size-Dependent Properties of [5]–[12]Cycloparaphenylenes

SCHOLARONE™
Manuscripts

Journal Name

ARTICLE

The Dynamic, Size-Dependent Properties of [5]-[12]Cycloparaphenylenes

Evan R. Darzi and Ramesh Jasti

[n]Cycloparaphenylenes (or "carbon nanohoops") are cyclic fragments of carbon nanotubes that consist of n *para* linked benzene rings. These strained, all sp^2 hybridized macrocycles, have size-dependent optical and electronic properties that are the most dynamic at the smallest size regime where n = 5-12. This review highlights the unique physical phenomena surrounding this class of polycyclic aromatic hydrocarbons, specifically emphasizing the novel structural, optical, and electronic properties of [5]-[12]CPPs.

Key Learning Points

(1) [n]CPPs have a narrowing HOMO-LUMO gap as the number of benzene rings n decreases. This trend is contrary to linear [n]paraphenylenes and most other conjugated macromolecules which have a narrowing HOMO-LUMO gap as n and conjugation length is increased.

(2) Strain induces torsional angle minimization as nanohoops become smaller. This torsional angle minimization leads to an effective increase in conjugation length for smaller sizes.

(3) HOMO-LUMO optical transitions are Laporte forbidden due to a conservation of orbital symmetry for the centrosymmetric CPPs. Absorbance maxima for all [n]CPPs are virtually identical and can be attributed to nearly degenerate HOMO-1 to LUMO or HOMO-2 to LUMO transitions, and HOMO to LUMO+1 or HOMO to LUMO+2 transitions.

(4) Fluorescence is red-shifted and quantum efficiency decreases as nanohoops become smaller. This phenomenon is accounted for by a violation of the Frank-Condon principal resulting in the relaxation from S_2 and S_3 states to geometrically relaxed $S_{1'}$ state. In larger [n]CPPs (where $n \geq 7$) the $S_{1'}$ state breaks the symmetry of the ground state causing emission to the S_0 state with decreasing quantum efficiency and redshifting fluorescence from [12]CPP to [7]CPP. In smaller [n]CPPs (where $n \leq 6$) the $S_{1'}$ state conserves the symmetry of the ground state and so emission to the S_0 state is forbidden and no fluorescence is observed.

(5) [n]CPPs organize in the solid state with long range channels and sub van der Waals radius intermolecular carbon-carbon interactions.

Synthetic chemists often pursue structurally unique molecules in anticipation that these unexplored architectures might impart physical properties that are not present in more common motifs.[1] The field of polycyclic aromatic hydrocarbon (PAH) chemistry is rich with examples, commencing with the historic work in the field by Kekule in 1865 when he first elucidated the cyclic six electron aromatic structure of benzene.[2] In more recent years, curved and distorted nonplanar PAHs have attracted significant attention from the scientific community in that these structures push the boundaries of our understanding of aromaticity and electron delocalization.
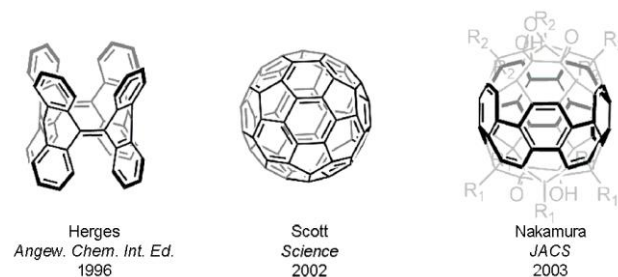

Herges
Angew. Chem. Int. Ed.
1996

Scott
Science
2002

Nakamura
JACS
2003

Figure 1: Inspirational bottom up syntheses of curved PAHs.

(5,5) CNT

[5]CPP
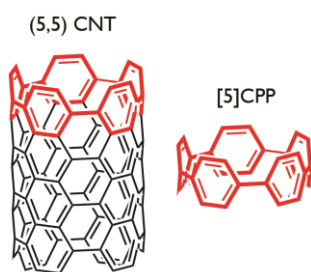
Figure 2: [n]CPPs are fragments of (n,n) armchair CNTs.

Buckminsterfullerenes and carbon nanotubes (CNTs) have drawn special interest due to their unprecedented material properties and promise in the field of nanotechnology. Pioneers such as Herges with the synthesis of the picotube, Scott with the bottom-up synthesis of C_{60}, and Nakamura with the synthesis of a caged acene belt (Fig. 1) have paved the way for the rational synthesis of new PAHs that continue to push the frontiers of our understanding of these unique structures.[3-5]

The [n]cycloparaphenylenes ([n]CPPs), which can be envisioned as the shortest cross-section of an [n,n] armchair CNT (Fig. 2), are a fascinating new class of PAHs due to their potential as seeds towards uniform armchair CNT growth.[6-8] The [n]CPPs were first envisioned (although not synthesized) by Parehk and Guha in 1933, many years before the discovery of CNTs.[9] Another 60 years passed until Vögtle examined synthetic routes to [n]CPPs.[10] Although he too was unsuccessful at preparing [n]CPPs, many of the proposed strategies laid the foundation for the eventual realization of the [n]CPPs in 2008 by Jasti and Bertozzi.[11] Since the first synthesis in 2008, [5]-[16]CPP, and [18]CPP have been accessed along with several substituted analogues.[11-30] Moreover, initial work has suggested that these molecular templates indeed have potential as controlling elements for CNT synthesis.[8]

In conjunction with their synthesis, numerous size-dependent properties of these molecules have been elucidated that are unique to this class of structures.[11, 19, 31-39] These properties are proving to be fascinating in their own right and promising for future materials science applications—aside from CPPs use as CNT templates. [n]CPPs have a narrowing HOMO-LUMO gap as the number of
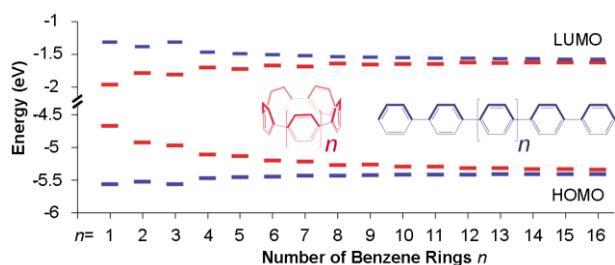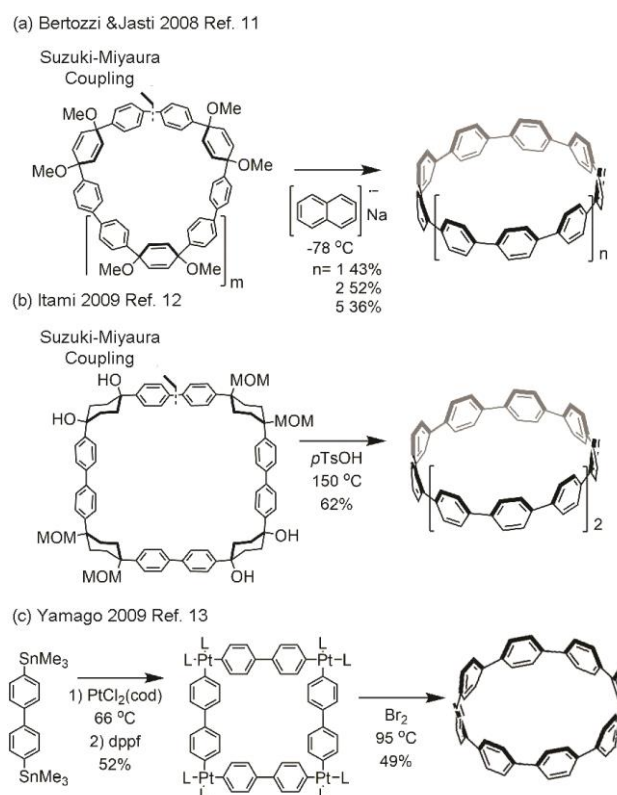
Figure 3: Linear paraphenylenes and most conjugated materials have a narrowing HOMO-LUMO gap as conjugation length increases. Cyclic paraphenylenes on the other hand show the opposite trend. Data taken from reference 19.

benzene rings, *n,* decreases.[19, 35] This is in direct contrast to the open chain linear paraphenylenes and most other conjugated materials which show narrowing HOMO-LUMO gaps with increased number of aromatic rings (Fig. 3).[40] In fact, [n]CPPs have more narrow HOMO-LUMO gaps than even the very longest linear paraphenylene highlighting their potential as new organic semiconducting materials. In addition, all [n]CPPs curiously share a common absorbance maximum while the emission is red-shifted as the hoop size decreases.[11, 19, 35, 41] These novel size-dependent optoelectronic properties are most dynamic in the smaller size regime of the [n]CPPs where *n* = 5-12. In this tutorial review, we highlight the unusual physical properties of CPPs in this smaller size regime, focusing on both experimental and theoretical data, and where applicable providing rationale for these unique physical properties.

Synthetic Approaches to [n]Cycloparaphenylenes

Synthetic approaches to the CPPs have been thoroughly discussed elsewhere, so we only provide a brief synopsis of strategies that led to the isolation of these structures. Although these molecules are structurally simple, the high strain energy of the non-planar benzene rings renders their synthesis challenging. The first synthesis of [n]CPPs was reported by Jasti and Bertozzi in 2008 yielding [9]-, [12]-, and [18]CPP in milligram quantities (Scheme 1a).[11] The key to this synthetic approach was the use of ridged 1,4-*syn*-dimethoxy-2,5-cyclohexadienes as masked benzene rings.[42] This appropriately substituted cyclohexadiene unit is able to alleviate strain and allow for

(a) Bertozzi &Jasti 2008 Ref. 11

Suzuki-Miyaura Coupling

(b) Itami 2009 Ref. 12

Suzuki-Miyaura Coupling

(c) Yamago 2009 Ref. 13

Scheme 1: General synthetic routes used to access [n]CPPs by (a) Jasti, (b) Itami, and (c) Yamago.

Suzuki-Miyaura cross-coupling/macrocyclization to macrocycles of varying size. In the final reductive aromatization step, these cyclohexadiene containing macrocycles are treated with lithium naphthalenide at −78 °C to reveal the fully benzenoid hoops. This synthetic strategy has since been extended and optimized to afford [5]-[12]CPP in a size selective and scalable manner.[11, 14-18]

In 2009, the Itami group introduced a slightly different approach to selectively synthesize [12]CPP (Scheme 1b).[12] This strategy utilized a substituted 1,4-*syn*-diarylcyclohexane units as a masked benzene ring to build low strain macrocyclic precursors.[10] It is worth noting that these cyclohexane units are reduced versions of benzene rings, where as the Jasti/Bertozzi cyclohexadiene approach uses oxidized versions of benzene rings. The low strain cyclohexane containing macrocycle was subsequently aromatized using *p*-toluenesulfonic acid at 150 °C which initiates an acid-catalysed dehydrogenation/oxidation event to reveal [12]CPP. Recent advances to this strategy include nickel mediated intramolecular reductive homocouplings of aryl bromides, which has led to higher yields and avoids the derivatization of aryl precursors to boronates. This strategy has been used to access [7]-[16]CPP in a size selective manner.[12, 24-26]

Later in 2009, the Yamago laboratory reported the first synthesis of [8]cycloparaphenylene using an entirely different approach (Scheme 1c).[13] This strategy relies on formation of a cyclic platinum complex followed by bromine-induced reductive elimination. Recent advances include the introduction of XeF_2 to induce reductive elimination to prepare even smaller [*n*]CPPs.[21] This route has been utilized to access [6]CPP and [8]-[13]CPP in relatively short synthetic sequences and high yields.[13, 19-22] In summary, due to the pioneering work of several groups, a new class of PAHs that remained dormant for decades is now synthetically accessible.

Structural Features of [*n*]Cycloparaphenylenes

The subtle interplay of strain, geometry, and symmetry plays a significant role in many of the interesting properties of [*n*]CPPs. Intuitively, strain energy increases as the nanohoops become smaller. Itami and coworkers nicely quantified this relationship using a series of homodesmotic reactions at the B3LYP/6-31G(d) level of theory to estimate the strain of [5]-[12]CPP.[18, 43] As seen in Table 1, the strain increases dramatically with smaller sized [*n*]CPPs. [12]Cycloparaphenylene, the largest in the series presented, has a sizable 48 kcal/mol of strain energy which equates to approximately 4 kcal/mol per aryl ring. [5]CPP at the other end of this size regime has an estimated 119 kcal/mol of strain energy spread out over only five aryl rings. This works out to nearly 24 kcal/mol of strain energy per benzene ring! As a frame of reference the highly strained hydrocarbon cubane was shown to have approximately 169 kcal/mols of strain estimated by a similar computational method.[44]

Table 1: Calculated B3LYP/6-31G(d) total strain, strain per benzene ring, displacement angle, and diameter of [5]-[12]CPP.

[n]CPP	Calculated Strain (kcal/mol)	Average Strain Per Aryl Ring (kcal/mol)	a° (degrees)	Diameter (nm)
5	119[a]	24	15.8	0.67[a]
6	97[b]	16	12.6	0.79[b]
7	84[b]	12	10.9	0.95[b]
8	72[b]	9	9.3	1.1[b]
9	66[b]	7	8.3	1.2[b]
10	58[b]	6	7.7	1.4[b]
11	54[b]	5	6.8	1.5[b]
12	48[b]	4	6.2	1.6[b]

[a] Reference 18. [b] Reference 43.

As studied by DFT calculations, nanohoop size plays a key role in the geometry and conformation of these nanohoops (Fig. 4).[35, 39, 41, 43, 45] As cycloparaphenylene size decreases, torsional angle Θ become smaller to compensate for the increasing strain energy.[35, 45] The minimization of these angles gives rise to better pi overlap and an effective increase in the conjugation between neighbouring aryl rings for smaller nanohoops. Increased conjugation due to smaller torsional angles offers one possible explanation (or at least contributing factor)
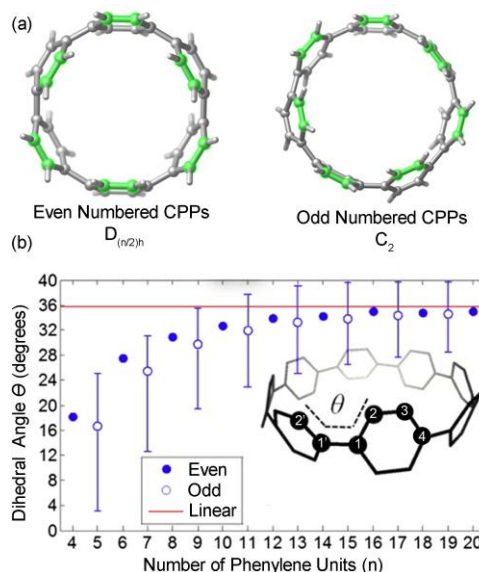

Figure 4: Point group of (a) even n = 6, 8, 10, and 12 and odd n = 5, 7, 9, 11 [*n*]CPPs. (b) Torsional angle Θ of cyclic and linear paraphenylenes. Reproduced with permission. Copyright © Elsevier

for the observed narrowing of the HOMO-LUMO gap as

cycloparaphenylenes become smaller.[39] In contrast, linear paraphenylenes, regardless of size, display a conformation in which the torsional angle is consistently 36° (Fig. 4, red line) — presumably the right balance between avoiding C-H/C-H steric interactions and maximizing *pi* overlap.[45] Further subtle effects can be observed when comparing conformations of cycloparaphenylenes with an odd number of benzene rings with those with an even number of benzene rings.[19, 39] Nanohoops having an even number of benzene rings ($n = 4, 6, 8, 10,$ and 12) have $D_{(n/2)h}$ symmetry with constant torsional angles and an alternating canted aryl-aryl orientation around the hoop (Fig. 4a).[43, 45] The increasing strain of smaller hoops leads to a drop in average torsional angle from approximately 34° for [12]CPP down to 28° for [6]CPP.[45] Odd sixed nanohoops ($n = 5, 7, 9,$ and 11) cannot achieve this alternating structure and instead have C_2 symmetry with a range of torsional angles and always one aryl ring perpendicular to the plane of the hoop creating a helical twist in the minimized geometry (Fig. 4a).[43, 45] The increase in strain energy down the odd series leads to a drop in average torsional angle from 32° ([11]CPP) down to 16° ([5]CPP).[45] The average torsional angles for [n]CPPs
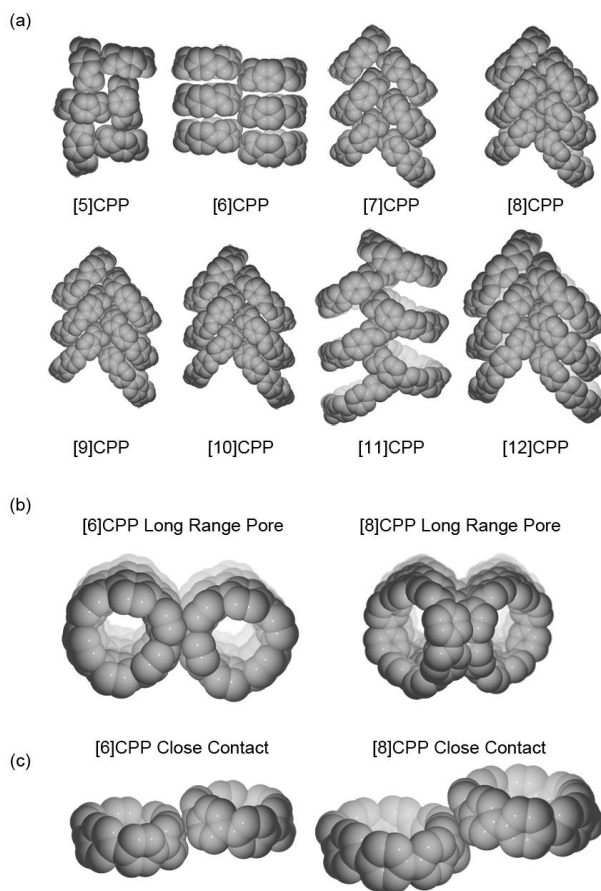

Figure 5: Crystal packing of [5]-[12]CPP in the solid state. (a) Side on view of crystal packing mode. (b) Top down view of [6]CPP and [8]CPP illustrating the long range channel present in [6]-[12]CPP. (c) Close intermolecular interactions found in [6]CPP and [8]CPP crystal structures.

where $n \geq 12$ reach a steady state nearly equal to those adopted by linear paraphenylenes, again highlighting the uniqueness of smaller [n]CPPs where $n \leq 12$ (Fig. 4b).

Analysis of crystal structures can provide additional insight into the interesting properties and potential solid state application of [n]CPPs. Crystal structures of [5]-[10]CPP, and [12]CPP have all been published in the primary literature.[13, 15, 16, 18, 20, 23, 24, 26] To complete this series we have contributed the structure for [11]CPP for the purpose of this review (CCDC deposition number for [11]CPP 1035794). Figure 5 illustrates the solid state structures of [5]-[12]CPP. Solvent molecules are typically present in the cavity of these structures but are often disordered and/or partially missing. For the purpose of clarity, solvent molecules have been removed from these depictions. X-ray crystallography allows us to probe a variety of geometric features of interest. As a benzene ring becomes more increasingly nonplanar, a point should arise when the structure can no longer maintain delocalization and therefore aromaticity. A 2003 computational paper suggested a transition from benzenoid to quinoid electronic structures occurring between [6]CPP and [5]CPP, with [5]CPP being completely quinoidal.[46] A close analysis of the solid state structure of [5]CPP revealed that the C_1-C_2 and C_2-C_3 bond lengths (see Fig. 4b for atom numbering) were nearly equivalent for all rings in the hoop, consistent with a benzenoid structure.[18] Crystal structure of the cycloparaphenylenes also allow for the analysis of the average ring displacement for the different sized nanohoops (Table 1). For a frame of reference, the highly distorted aryl ring in the natural product haouamine A, first synthesized by Baran[47], has a displacement of 13.6°, [2,2]paracyclophane has a displacement of 14.1°[48], and a [1.1]paracyclophane[49] adduct crystallized by Kawai and Tsuji has an impressive 25.6° displacement. [5]CPP, the smallest CPP synthesized to date, has an average displacement angle of 15.6° (for all five rings) and an astounding 119 kcal/mol of strain energy! The next CPP in the series yet to be synthetically accessed is [4]CPP and is predicted to have 146.8 kcal/mol of strain and an average displacement angle of 19.4° highlighting the increasing synthetic challenge with smaller nanohoops.

In addition to the measurements above, X-ray crystallography allows us to examine the solid state packing structures of CPPs. [5]CPP and [7]-[12]CPP all adopt a herringbone packing structure. [5]CPP shows an especially dense packing with no solvent in the pore of the hoop due to the small cavity size. Each CPP molecule is perfectly nested perpendicular to the plane of all neighbouring molecules in the lattice. [11]CPP also shows a unique flavour of herringbone packing. Here each ring is nested inside the pore of its two closest neighbours. [6]CPP provides the most aesthetically striking and unique packing out of the series. The [6]CPP molecules stack perfectly on top of one another, somewhat reminiscent of an armchair CNT (Fig. 5a). To date no crystalline polymorphs of any [n]CPP have been reported. Attempts in our laboratory to obtain a crystal of [5]-, or [7]-[12]CPP with columnar packing or [6]CPP with herringbone packing has not been achieved. All [n]CPPs except [5]CPP have a long range channel in the solid state which is often occupied by solvent. Two representative examples, [6]CPP and [8]CPP are shown in figure 5b by a 90° rotation perpendicular to the

page from the side on packing illustrated in Fig. 5a. Finally, each [*n*]CPP has close intermolecular C-C contacts within 3.5 Å. Figure 5c illustrates a representative example of this interaction for [6]CPP and [8]CPP. The combination of the packing structures, the long range pores, and close intermolecular contacts make [*n*]CPPs an intriguing candidate for many electronic applications including small molecule sensing, organic field effect transistors (OFETs), or organic photovoltaic devices.

Nuclear Magnetic Resonance Spectroscopy of [*n*]CPPs

Nuclear magnetic resonance (NMR) spectroscopic data for [5]-[12]CPP provides further experimental evidence in regards to the conformation of CPPs and their dynamics. The proton NMR spectra of [5]-[12]CPP (Fig. 6a) each exhibit one singlet peak suggesting all protons in each CPP molecule are in a similar environment on the NMR timescale.[11] This equivalency can be explained by rapid wobbling and/or canting motions where individual benzene rings slip past one another. Itami[43] and co-workers calculated the activation barrier for this canting motion for [12]CPP as 3.7 kcal/mol. A second type of fluctuation where benzene rings flip through the centre of the hoop would also lead to an equivalency in the NMR. This process was estimated to have an activation barrier of 7.5 kcal/mol for [12]CPP. Although these calculations have not been reported for smaller sized CPPs, as the hoop becomes smaller and the strain energy is increased,

a full flip of a benzene ring through the centre of the hoop will become more difficult.[15, 18]

The signal in the ^{1}H NMR spectra of [12]-[8]CPP shows a consistent upfield shift as CPP size gets smaller. [7]-[5]CPP, however, show the opposite trend and their proton signal shifts downfield as CPP size decreases (Fig. 6a). As shown in Figure 6b and 6c, each [*n*]CPP has two distinct carbon signals, where all C_{ortho} carbons (Fig. 6b) are equivalent and all C_{ipso} carbons (Fig. 6c) are equivalent. The signal for the C_{ortho} carbon shifts downfield moving from [12]CPP to [8]CPP and abruptly shifts upfield from [7]CPP to [5]CPP. One possible explanation for these trends is that as the nanohoops become smaller, the torsional angles minimize and thus the ^{1}H and C_{ortho} [13]C signals follow the patterns of the bay regions of extended PAHs. For example, the bay region ^{1}H signals in phenanthrene shift downfield relative to benzene whereas the ^{13}C NMR shift upfield. These observations have been rationalized by a ring current effect where the proton in the bay region lies perpendicular to the pi system in a deshielding region. The bay region protons are also locked in an eclipsed conformation resulting in a shift of some electron density from the proton onto the attached carbon.[50] In contrast to the proton
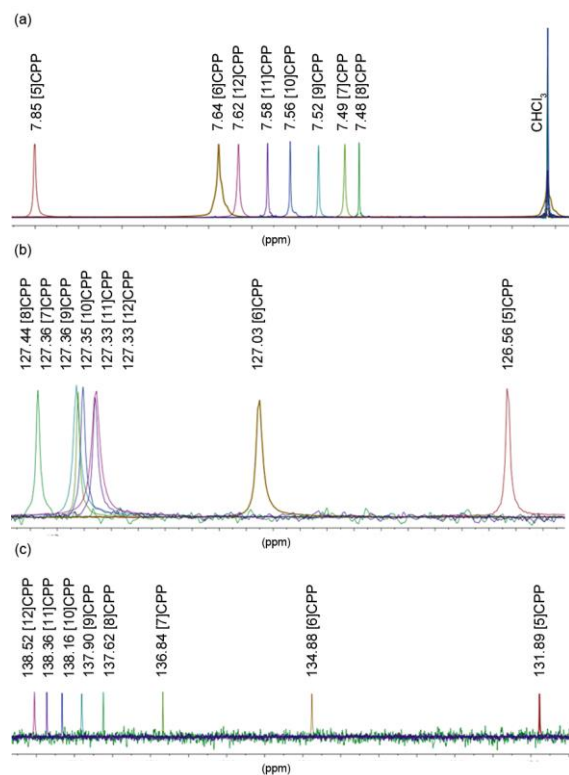

Figure 6: (a) ^{1}H NMR spectra of [5]-[12]CPP, (b) ^{13}C spectra of C_{ortho} for [5]-[12]CPP, and ^{13}C spectra of C_{ipso} for [5]-[12]CPP.

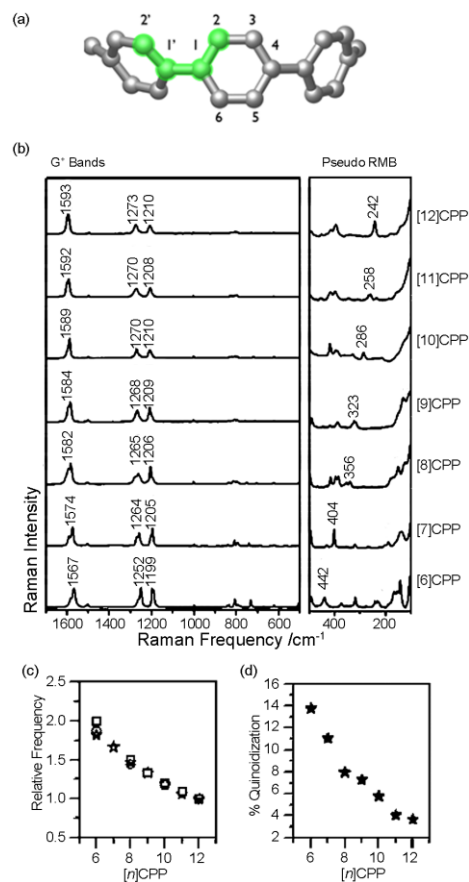

Figure 7: (a) Representative [n]CPP bonds and torsional angle highlighted in green. (b) Raman spectra of [6]-[12]CPP (c) Raman frequency vs [*n*]CPP and (d) percent quinoidization vs [*n*]CPP. Reproduced with permission. Copyright © Wiley

and the C_{ortho} carbon, the C_{ipso} carbons show a gradual shift upfield consistent with an increasing pyramidalization of this carbon.

Raman Spectroscopy of [*n*]CPPs

Raman spectroscopy has proven to be an indispensable tool for characterizing CNTs. Due to CNTs' polymeric nature and high molecular weights, traditional spectroscopies such as NMR, IR, and mass spectrometry provide limited insight into CNT structure. For CNTs, three major Raman modes are used to characterize the diameter and chirality of the nanotube. G^+ bands correlate motions perpendicular to the length of the tube, G^- bands are related to motions parallel to the tube, and radial breathing modes (RBMs) are a result of the expanding and contracting of the tube. Several labs have recently reported the Raman spectra of [*n*]CPPs offering an experimental glimpse into the structural details of these nanohoops.[45, 51, 52]

The Casado[51] group has reported on the Raman spectroscopy of [6]-[12]CPP, offering perhaps the most complete and resolved data to date (Fig. 7). A pseudo RBM peak was assigned to minor peaks falling between 200 and 500 cm^{-1} (Fig. 7b). As the hoop becomes smaller and more rigid, the peaks shift to higher wavenumbers. Like CNTs, [*n*]CPPs show a linear relationship between the frequency and the reciprocal of the nanohoop diameter (1/d) establishing this peak as a fingerprint for nanohoop diameter. [*n*]CPPs, like CNTs, have G^+ bands between 1500 and 1600 cm^{-1} that can be assigned to totally symmetric vibrations parallel to the plane of the hoop ($C_{1-1', 2-3, and 5-6}$) (Fig. 7b). This band was used to experimentally probe the percent quinoidization of each hoop. A flat benzene ring was calculated to have a peak at 1600 cm^{-1} while a quinoidal ring was predicted to be at a lower wavenumbers of 1343 cm^{-1}. As the hoops become smaller, this signal shifts to lower wavenumbers and thus these smaller hoops have more quinoidal character, which is also supported by crystal structure data (*vida supra*) (Fig. 7c). Figure 7d shows the empirical percent quinoidization of each nanohoop which closely follows the trends calculated for strain energy. [12]CPP was found to have 3% quinoid character while [6]CPP was found to have nearly 14% quinoid character implying a gradual quinoidization as the hoops become smaller.

The Casado[51] group has also shown how Raman spectroscopy can provide a unique tool to describe the effect of pressure on [n]CPPs (Fig. 8). Raman spectra were recorded independently for [12]CPP and [6]CPP at ambient pressure and 8GPa. [12]CPP showed a pressure induced shift of the G^+ mode indicative of partial planarization of a segment giving it more benzenoid character. Upon release of this pressure the signal rebounded to the ambient state suggesting a reversible flexing of the hoop under pressure (Fig. 8b). [6]CPP also showed significant distortion of the G^+ mode under 8GPa, however, the signals did not recover upon release of pressure representative of an irreversible collapse of the structure (Fig. 8a). When a solid matrix of [12]CPP and [6]CPP were pressurized together, both the [12]CPP and [6]CPP signals were recovered. This was attributed to a pressure induced host guest complex of [6]CPP@[12]CPP where the [12]CPP acts to shield the [6]CPP from irreversible collapse. This complex is the first experimental observations of such ring in ring complexation reminiscent of multi-walled CNTs (Fig. 8c). Next the host guest

complex of C_{60}@[10]CPP was examined under 6GPa of pressure. First, a Raman spectrum was measured individually for [10]CPP, C_{60}, the radical cation [10]CPP$^{•+}$, and the radical anion $C_{60}^{•-}$. Next a Raman spectrum was measured for the complex C_{60}@[10]CPP at ambient
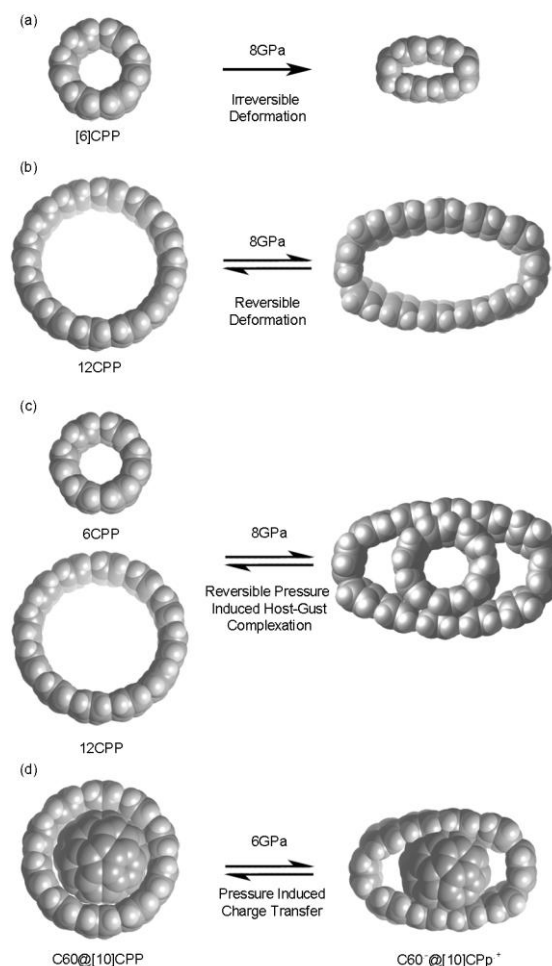

Figure 8: Cartoon of the pressure induced (a) irreversible deformation of [6]CPP (b) reversible deformation of [12]CPP (c) reversible host guest complexation of [6]CPP@[12]CPP and (d) charge transfer from [10]CPP to C_{60}.

pressure and 6GPa. Analysis of these spectra showed that upon application of pressure the [10]CPP signal shifted from 1588 cm^{-1} (neutral compound) to a signal consistent with a radical cation [10]CPP$^{•+}$ at 1569 cm^{-1}. Accompanying these dynamic shifts the neutral C_{60} signal shifted from 1469 cm^{-1} 1463 cm^{-1} indicating the formation of the radical anion $C_{60}^{•}$. These signals recovered to the neutral C_{60}@[10]CPP when pressure was released suggesting a pressure induced charge transfer event where an electron from the electron rich [10]CPP is given to the electron accepting C_{60} under high pressures (Fig. 8d). The application of pressure to induce a charge transfer event between the electron rich nanohoop to the electron poor fullerene highlights a potential novel materials application of these molecules.

Electrochemistry

Table 2: Published oxidation and reduction potentials of [*n*]CPPs (V vs Fc/Fc$^+$).

[*n*]CPP	Oxidation (V)	Reduction (V)
5	0.25*[a], 0.46*[a]	-2.27*[a], -2.55*[a]
6	0.44[b], 0.30[c]	NA
7	0.55[d]	-2.74[d]
8	0.59[e]	NA
9	0.70[e]	NA
10	0.74[e]	NA
11	0.83[e]	NA
12	0.85[e]	NA

[a] Reference 18. [b] Reference 15. [c] Reference 21. [d] Reference 39. [e] Reference 19. *Indicates pseudo reversible wave.

Cyclic voltammetry has provided the clearest experimental observation of the lowering LUMO and raising HOMO energy as [*n*]CPP size decreases. Oxidation potentials for [5]-[12]CPP and reduction potentials for [5]CPP and [7]CPP have been reported in the literature (Table 2).[15, 18, 19, 21, 39] Although the experimental conditions for the electrochemical experiments are not completely uniform, the nanohoops clearly become easier to reduce and oxidize as the hoop become smaller. Oxidation waves for [5]-[12]CPP demonstrate that as the nanohoops becomes smaller, removal of one electron becomes more facile indicative of a higher energy HOMO. [12]CPP[19] for example has a half-wave potential of 0.85 V vs Fc/Fc$^+$ while [6]CPP[15] has a half-wave potential of 0.44 V vs Fc/Fc$^+$. Interestingly, [5]CPP[18] uniquely shows two pseudo reversible oxidations at peak potentials of

0.25 and 0.46 V vs Fc/Fc$^+$. Reduction waves are only reported for [5]CPP[18] and [7]CPP, but illustrate that as the hoop becomes smaller the reductions become more facile indicative of a lowering of the LUMO. Again, [5]CPP shows two pseudoreversible reduction peaks with peak potentials at −2.27 and −2.55 V vs Fc/Fc$^+$ while [7]CPP shows only one reversible peak with a half-wave potential of −2.74 V vs Fc/Fc$^+$.
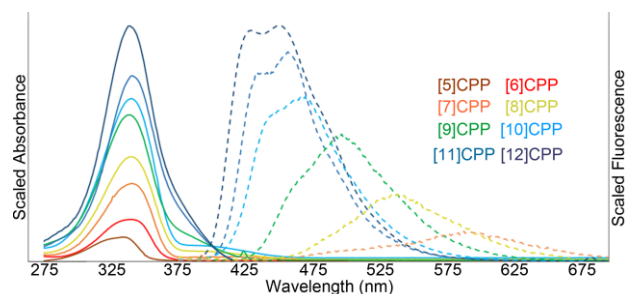
Carbon Nanohoop Photophysics

Figure 9: UV/VIS (solid) and fluorescence (dashed) spectra for [5]-[12]CPP. No fluorescence is observed for [6]CPP or [5]CPP.

The unique photophysics of the nanohoop structures have been well appreciated since the inception of [*n*]CPPs. Table 3 shows a collection of all the absorbance and fluorescence data while Figure 9 shows an overlay of [5]-[12]CPP absorbance and fluorescence spectra.[11, 17, 19, 35, 39, 52a-c] A number of striking features for this homologous series are apparent from this data. First, [5]-[12]CPP have a common absorbance with maxima between 348- 350nm. An explanation for this observation was postulated by the Yamago[19] group using time dependent density function theory (TD-DFT). Due

Table 2: Summary of experimental photophysical properties for [5]-[12]CPP.

[n]CPP	Absorbance (nm)	Extinction coefficient ε (M^{-1} cm^{-1})	Fluorescence (nm)	Fluorescence Quantum Yield Φ	Singlet Lifetime (ns)	Transient Absorbance (nm)	Phosphorescence (nm)	Triplet Lifetime (ns)
5	335 [a,b]	5.7 x 10^4 [a]	No Fluorescence[a,b]	0 [a,b]	NA	NA	NA	NA
6	340 [c]	NA	No Fluorescence[c]	0 [c]	NA	NA	NA	NA
7	340 [d]	6.9 x 10^4 [l]	587 [d]	0.007 [d]	NA	NA	NA	NA
8	340 [e]	1.0 x 10^5 [h]	533 [e]	0.1[h]	17.6 [i]	708 [k], 400 [k]	671 [k]	60000 [k]
9	340 [f]	1.2 x 10^5 [h]	494 [f]	0.38 [h]	10.6 [i], 5.3 [j]	671 [k], 389 [k]	633 [k]	63000 [k], 67000 [j]
10	338 [g]	1.3 x 10^5 [h]	466 [g]	0.65 [h]	6.6 [i]	678 [k], 472 [k]	610 [k]	58000 [k]
11	340 [g]	1.3 x 10^5 [h]	458 [g]	0.73 [h]	3.8 [i]	676 [k], 487 [k]	600 [k]	64000 [k]
12	339 [f]	1.4 x 10^5 [h]	450 [f]	0.81 [d]	2.4 [i], 1.9 [j]	668 [k], 500 [k]	591[k]	64000 [k], 110000 [j]

[a] Reference 18. [b] Reference 22. [c] Reference 15. [d] Reference 14. [e] Reference 13. [f] Reference 6. [g] Reference 11. [h] Reference 17. [i] Reference 35. [j] Reference 52c. [k] Reference 52b. [l] Reference 39.
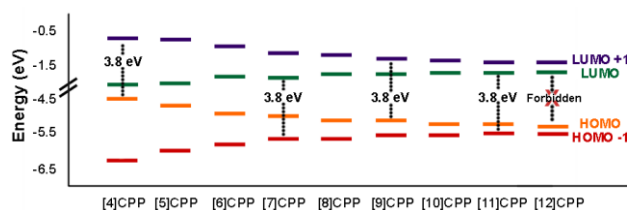
Figure 10: Calculated (B3LYP/6-31G) (d) HOMO, HOMO-1, LUMO, and LUMO+1 energy levels (B3LYP/6-31G*). HOMO-1 and HOMO-2 are nearly degenerate as are LUMO+1 and LUMO+2. For clarity purposes only HOMO-1 and LUMO+1 energies were used. Data taken from reference 19.

to the centrosymmetric nature of these nanohoops, the HOMO-LUMO transition is Laporte forbidden as the HOMO and LUMO conserve symmetry[35]. The HOMO-LUMO transition for even numbered CPPs has an oscillator strength of zero. The HOMO-LUMO transition for odd numbered nanohoops is non-zero due to the inherent lower symmetry, however the intensity is still very low. [5]-[12]CPP are shown to have degenerate HOMO-1/HOMO-2 and a nearly degenerate LUMO+1/LUMO+2. These orbitals have different symmetries than the HOMO and LUMO and so transitions from HOMO-1 or HOMO-2 to the LUMO are allowed. Likewise a transition from the HOMO to the LUMO+1 or LUMO+2 is also allowed. These distinct transitions have orthogonal transition dipole moments accounting for the relatively high extinction coefficients for all [n]CPPs (Table 3). The orbital energy trend for the HOMO-1/HOMO-2 and LUMO+1/LUMO+2 is opposite that of the HOMO and LUMO. Like linear paraphenylenes and other conjugated materials, these gaps narrow as the hoop becomes larger in stark contrast to the HOMO-LUMO gap which narrows as the hoop becomes smaller[40]. Figure 10 illustrates that the relative magnitude of the transition is conserved across the homologous series accounting for the common absorbance of [5]-[12]CPP.

While the absorbance trends can be easily understood computationally, the red-shifting fluorescence and rapid decrease in quantum efficiency with smaller nanohoops are more challenging to model. A number of theoretical papers have attempted to account for these observed properties.[31, 33, 34, 36-38, 41, 53] We have chosen to focus on the most recent report by Tretiak[33] since it offers a reasonable and clear explanation of both the observed red-shifting emission and drop in quantum efficiency of smaller nanohoops. According to Kasha's rule[54], fluorescence emission typically occurs from the lowest energy excited state S_1 to the ground state S_0. Due to the Laporte selection rules all [n]CPPs are initially excited to the S_2 and S_3 states through a combination of HOMO-LUMO+1 or HOMO-LUMO+2 and HOMO-1-LUMO or HOMO-2-LUMO transitions[19, 35]. Nonadiabatic excited state dynamics simulations were used to show that photoexcited S_2 and S_3 states are able to internally convert to spatial localized $S_{1'}$ states within 50 femtoseconds[33]. This internal conversion to the $S_{1'}$ state (fs timescale) is significantly faster than the experimental fluorescent lifetimes (ns timescale) giving support to this theory.[32, 35, 52c] Moreover, Tretiak shows that in larger [n]CPPs, where $n \geq 8$, the

lowest energy excited state geometry ($S_{1'}$) has partial planarization of five aryl rings leaving the rest of the hoop in the ground state geometry allowing self-trapping of the exitonic wave function (Fig.11). This localized $S_{1'}$ state has different symmetry from the ground state and thus becomes an allowed $S_{1'}$-S_0 transition. In smaller [n]CPPs, where $n \leq 7$, complete delocalization is observed in the lowest energy excited state geometry ($S_{1'}$) conserving the symmetry of the ground state. Therefore, this $S_{1'}$-S_0 transition conserves symmetry and is Laporte forbidden accounting for the rapid drop in quantum efficiencies of smaller nanohoops. As stated before, strain induces a decrease in torsional angle which in turn increases the amount of conjugation as nanohoops get smaller therefore enhancing vibrational coupling and reducing the $S_{1'}$-S_0 energy resulting in a gradual red-shifting of the fluorescence[33].
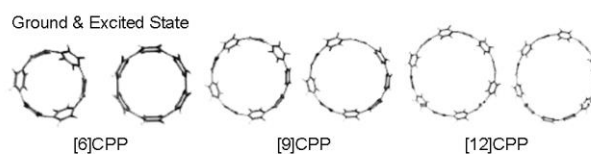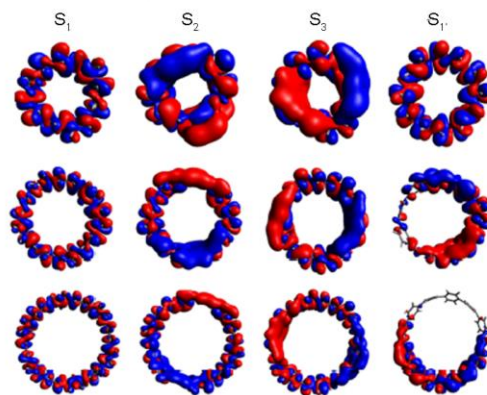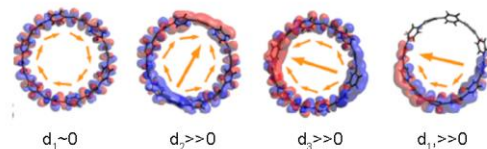

Figure 11: a) Minimized geometries of the ground state and first excited state. b) Orbital visualization of S_1, S_2, S_3, and $S_{1'}$ transitions. c) Transition dipole for [12]CPP illustrating the self-trapping $S_{1'}$ state. Reproduced with permission. Copyright © ACS

Conclusions

The new molecular family of [n]cycloparaphenylenes or "carbon nanohoops" is a prototypical example of how access to unprecedented architectures can lead to unexpected and unique physical properties.

These properties include the narrowing of the HOMO-LUMO gap in [*n*]CPPs as the hoop size decreases which is in direct contrast with typical conjugated macromolecules. This unique optoelectronic behaviour is in accordance with the strain induced decrease in torsional angle and ultimately the increase in conjugation for the smaller nanohoops. The inherent symmetry of these centrosymmetric molecules results in a Laporte forbidden HOMO-LUMO optical transition impacting both the absorbance and emission spectra. The common absorbance observed for [*n*]CPPs consists of nearly degenerate allowed HOMO to LUMO +1 and LUMO +2 and orthogonal HOMO -1 and HOMO -2 to LUMO optical transitions. A violation of the Frank-Condon principal[55] allows excited S_2 and S_3 states to relax to a localized $S_{1'}$ state. For [*n*]CPPs where n > 7, this $S_{1'}$ state has a different symmetry from the ground state resulting in an allowed $S_{1'}$ to S_0 transition. For [*n*]CPPs where n ≤ 7, the $S_{1'}$ state conserves the ground state symmetry resulting in a forbidden $S_{1'}$ to S_0 transition and thus a decrease in quantum yield in smaller nanohoops. Emission from the $S_{1'}$ state also accounts for the red-shifting fluorescence observed as nanohoops size decreases. The unique geometric features, solid state packing, and optoelectronic properties make [*n*]CPPs and their derivatives a fascinating candidate for many electronic applications including small molecule sensing, organic field effect transistors, and organic photovoltaic devices.

Acknowledgements

Notes and references

Department of Chemistry & Biochemistry and Material Science Institute, University of Oregon, Eugene, OR, 97403, USA

1. R. Hoffmann and H. Hopf, *Angew. Chem. Int. Ed.*, 2008, **47**, 4474-4481.
2. A. Kekuié, *Liebigs Ann.*, 1866, **137**, 129-196.
3. S. Kammermeier, P. G. Jones and R. Herges, *Angew. Chem. Int. Ed.*, 1996, **35**, 2669-2671.
4. E. Nakamura, K. Tahara, Y. Matsuo and M. Sawamura, *J. Am. Chem. Soc.*, 2003, **125**, 2834-2835.
5. L. T. Scott, M. M. Boorum and B. J. McMahon, *Science*, 2002, **295**, 1500-1503.
6. R. Jasti and C. R. Bertozzi, *Chem. Phys. Lett.*, 2010, **494**, 1-7.
7. E. H. Fort, P. M. Donovan and L. T. Scott, *J. Am. Chem. Soc.*, 2009, **131**, 16006-16007.
8. H. Omachi, T. Nakayama, E. Takahashi, Y. Segawa and K. Itami, *Nat. Chem.*, 2013, **5**, 572-576.
9. V. C. G. Parekh, P. C., *J. Indian. Chem. Soc.*, 1934, **11**, 95-100.
10. R. Friederich, M. Nieger and F. Vögtle, *Chem. Ber.*, 1993, **126**, 1723-1732.
11. R. Jasti, J. Bhattacharjee, J. B. Neaton and C. R. Bertozzi, *J. Am. Chem. Soc.*, 2008, **130**, 17646-17647.
12. H. Takaba, H. Omachi, Y. Yamamoto, J. Bouffard and K. Itami, *Angew. Chem. Int. Ed.*, 2009, **48**, 6112-6116.
13. S. Yamago, Y. Watanabe and T. Iwamoto, *Angew. Chem. Int. Ed.*, 2010, **49**, 757-759.
14. T. J. Sisto, M. R. Golder, E. S. Hirst and R. Jasti, *J. Am. Chem. Soc.*, 2011, **133**, 15800-15802.
15. J. Xia and R. Jasti, *Angew. Chem. Int. Ed.*, 2012, **51**, 2474-2476.
16. J. Xia, J. W. Bacon and R. Jasti, *Chem. Sci.*, 2012, **3**, 3018-3021.
17. E. R. Darzi, T. J. Sisto and R. Jasti, *J. Org. Chem.*, 2012, **77**, 6624-6628.
18. P. J. Evans, E. R. Darzi and R. Jasti, *Nat. Chem.*, 2014, **6**, 404-408.
19. T. Iwamoto, Y. Watanabe, Y. Sakamoto, T. Suzuki and S. Yamago, *J. Am. Chem. Soc.*, 2011, **133**, 8354-8361.
20. E. Kayahara, Y. Sakamoto, T. Suzuki and S. Yamago, *Org. Lett.*, 2012, **14**, 3284-3287.
21. E. Kayahara, T. Iwamoto, T. Suzuki and S. Yamago, *Chem. Lett.*, 2013, **42**, 621-623.
22. E. Kayahara, V. K. Patel and S. Yamago, *J. Am. Chem. Soc.*, 2014, **136**, 2284-2287.
23. Y. Segawa, S. Miyamoto, H. Omachi, S. Matsuura, P. Šenel, T. Sasamori, N. Tokitoh and K. Itami, *Angew. Chem. Int. Ed.*, 2011, **50**, 3244-3248.
24. Y. Segawa, Scaron, P. enel, S. Matsuura, H. Omachi and K. Itami, *Chem. Lett.*, 2011, **40**, 423-425.
25. Y. Ishii, Y. Nakanishi, H. Omachi, S. Matsuura, K. Matsui, H. Shinohara, Y. Segawa and K. Itami, *Chem. Sci.*, 2012, **3**, 2340-2345.
26. F. Sibbel, K. Matsui, Y. Segawa, A. Studer and K. Itami, *Chem. Commun.*, 2014, **50**, 954-956.
27. H. Omachi, Y. Segawa and K. Itami, *Org. Lett.*, 2011, **13**, 2480-2483.
28. S. Hitosugi, W. Nakanishi, T. Yamasaki and H. Isobe, *Nat. Commun.*, 2011, **2**, 492.
29. A.-F. Tran-Van, E. Huxol, J. M. Basler, M. Neuburger, J.-J. Adjizian, C. P. Ewels and H. A. Wegner, *Org. Lett.*, 2014, **16**, 1594-1597.
30. C. Huang, Y. Huang, N. G. Akhmedov, B. V. Popp, J. L. Petersen and K. K. Wang, *Org. Lett.*, 2014, **16**, 2672-2675.
31. M. Fujitsuka, D. W. Cho, T. Iwamoto, S. Yamago and T. Majima, *Phys. Chem. Chem. Phys.*, 2012, **14**, 14585-14588.
32. M. Fujitsuka, C. Lu, T. Iwamoto, E. Kayahara, S. Yamago and T. Majima, *J. Phys. Chem. A*, 2014, **118**, 4527-4532.
33. L. Adamska, I. Nayyar, H. Chen, A. K. Swan, S. Oldani, S. Fernandez-Alberti, M. R. Golder, R. Jasti, S. K. Doorn and S. Tretiak, *Nano Lett.*, 2014, **14**, 6539-6546.
34. V. S. Reddy, C. Camacho, J. Xia, R. Jasti and S. Irle, *J. Chem. Theory Comput.*, 2014, **10**, 4025-4036.
35. Y. Segawa, A. Fukazawa, S. Matsuura, H. Omachi, S. Yamaguchi, S. Irle and K. Itami, *Org. Biomol. Chem.*, 2012, **10**, 5979-5984.
36. T. Nishihara, Y. Segawa, K. Itami and Y. Kanemitsu, *J. Chem. Phys. Lett.*, 2012, **3**, 3125-3128.
37. C. Camacho, T. A. Niehaus, K. Itami and S. Irle, *Chem. Sci.*, 2013, **4**, 187-195.
38. T. Nishihara, Y. Segawa, K. Itami and Y. Kanemitsu, *Chem. Sci.*, 2014, **5**, 2293-2296.
39. P. Li, T. J. Sisto, E. R. Darzi and R. Jasti, *Org. Lett.*, 2014, **16**, 182-185.
40. M. Banerjee, R. Shukla and R. Rathore, *J. Am. Chem. Soc.*, 2009, **131**, 1780-1786.
41. B. M. Wong, *J. Phys. Chem. C*, 2009, **113**, 21921-21927.
42. M. Srinivasan, S. Sankararaman, H. Hopf and B. Varghese, *Eur. J. Org. Chem.*, 2003, **2003**, 660-665.
43. Y. Segawa, H. Omachi and K. Itami, *Org. Lett.*, 2010, **12**, 2262-2265.
44. X.-W. Fan, X.-H. Ju, Q.-Y. Xia and H.-M. Xiao, *J. Hazard. Mater.*, 2008, **151**, 255-260.
45. H. Chen, M. R. Golder, F. Wang, R. Jasti and A. K. Swan, *Carbon*, 2014, **67**, 203-213.
46. M. N. Jagadeesh, A. Makur and J. Chandrasekhar, *J. Mol. Modeling*, 2000, **6**, 226-233.
47. N. Z. Burns, I. N. Krylova, R. N. Hannoush and P. S. Baran, *J. Am. Chem. Soc.*, 2009, **131**, 9172-9173.
48. H. Hope, J. Bernstein and K. N. Trueblood, *Acta Crystallog. Sec. B*, 1972, **28**, 1733-1743.
49. T. Tsuji, M. Ohkita, T. Konno and S. Nishida, *J. Am. Chem. Soc.*, 1997, **119**, 8425-8431.
50. H. Friebolin, *Basic One- and Two Dimensional NMR Spectroscopy*, 3 edn., WILEY-VCH New York, 1998.

51.   M. P. Alvarez, P. M. Burrezo, M. Kertesz, T. Iwamoto, S. Yamago, J. Xia, R. Jasti, J. T. L. Navarrete, M. Taravillo, V. G. Baonza and J. Casado, *Angew. Chem. Int. Ed.*, 2014, **53**, 7033-7037.
52.   a) M. Fujitsuka, T. Iwamoto, E. Kayahara, S. Yamago and T. Majima, *ChemPhysChem*, 2013, **14**, 1570-1572. b) M. Fujitsuka, S. Tojo, T. Iwamoto, E. Kayahara, S. Yamago and T. Majima, *J. Phys. Chem. Lett.*, 2014, **5**, 2302-2305. c) D. A. Hines, E. R. Darzi, R. Jasti and P. V. Kamat, *J. Phys. Chem. A*, 2014, **118**, 1595-1600.
53.   D. Sundholm, S. Taubert and F. Pichierri, *Phys. Chem. Chem. Phys.*, 2010, **12**, 2751-2757.
54.   M. Kasha, *Discuss. Faraday Soc.*, 1950, **9**, 14-19.
55.   E. U. Condon, *Phys. Rev.*, 1928, **32**, 858-872.